

# Structural changes induced by cation ordering in ferrotapiolite

M. ZEMA\*, S. C. TARANTINO AND A. GIORGANI

Dipartimento di Scienze della Terra, Università di Pavia, Via Ferrata 1, 27100 Pavia, Italy

## ABSTRACT

Structural modifications as a function of the degree of order ( $Q$ ) in  $\text{FeTa}_2\text{O}_6$  ferrotapiolite have been characterized by means of single-crystal X-ray diffraction (SC-XRD). A total of 26 datasets covering the range of  $Q$  between 0.154 and 1 have been obtained by thermal treatments followed by quenching of natural tapiolite crystals. Ordering of  $\text{Fe}^{2+}$  at the  $A$  sites and of  $\text{Ta}^{5+}$  at the  $B$  sites causes a linear increase in the  $a/c$  lattice constants ratio, as a consequence of a linear decrease of the  $c$  dimension and only slight modifications of the  $a$  parameter. Calibration of  $a/c$  vs.  $Q$  represents a very useful tool for a rapid determination of the degree of order of tapiolite samples. Polyhedral volumes of the two octahedral sites vary linearly with  $Q$  as a consequence of the different ionic radii of the two species. Both the sites remain almost regular at all  $Q$  values but the  $B$  site shows an increasing off-centre displacement of the cation with increasing  $Q$ . Observed structure factors of supercell reflections, characterized by  $l \neq 3n$ , increase linearly as a function of  $Q$ , thus representing a further tool for a quick evaluation of the degree of order.

**KEYWORDS:** tapiolite, order-disorder, single-crystal X-ray diffraction.

## Introduction

THE mineral ferrotapiolite,  $\text{FeTa}_2\text{O}_6$ , crystallizes with the trirutile structure in space group  $P4_2/mnm$  (Fig. 1). In its crystal structure, long-range order-disorder occurs between  $\text{Fe}^{2+}$  and  $\text{Ta}^{5+}$  in the two octahedral sites  $A$  and  $B$ , with  $\text{Fe}^{2+}$  preferring the  $A$  site and  $\text{Ta}^{5+}$  preferring the  $B$  site. This is a convergent order-disorder process; random distribution of  $\text{Fe}^{2+}$  and  $\text{Ta}^{5+}$  cations between  $A$  and  $B$  sites results in the disordered rutile-type structure. The rutile and trirutile structures are related by an isomorphic transformation of index three, hence they have the same symmetry and the relationship between their unit cells is  $a_{\text{trirutile}} = a_{\text{rutile}}$  and  $c_{\text{trirutile}} = 3c_{\text{rutile}}$ . A thoughtful description of the different rutile-type derivatives was given by Baur (1994). The prominent feature of the tapiolite structure, which was solved by Goldschmidt (1926), is the presence of rows of edge-sharing octahedra that form straight chains running along the  $c$  direction. These chains show an  $\cdots ABBABB \cdots$  stacking

sequence where  $A$  represents  $\text{Fe}^{2+}$  and  $B$  represents  $\text{Ta}^{5+}$  in the ordered structure. Adjacent chains are joined together by shared corners of the octahedra.

Tapiolite minerals occur primarily as accessory phases in rare-element granitic pegmatites and are usually associated with other Nb,Ta-bearing minerals such as columbite-tantalite or wodginite. They are commonly characterized by limited substitution of  $\text{Ta}^{5+}$  with  $\text{Nb}^{5+}$  (<10%  $\text{Nb}_2\text{O}_5$ ) and of  $\text{Fe}^{2+}$  with  $\text{Mn}^{2+}$  (<2%  $\text{MnO}$ ). Natural tapiolite samples often show a certain degree of cation disorder. Nevertheless, to our knowledge, there are no data in the literature for order degrees of tapiolites and an accurate method for a quantitative determination of the degree of order in tapiolite has not yet been derived. Wise and Černý (1996), who gave a thorough description of the crystal chemistry of minerals of the tapiolite series with particular regard to the substitution of  $\text{Fe}^{2+}$  with  $\text{Mn}^{2+}$ , stated qualitatively, on the basis of a comparison of the unit-cell dimensions of untreated and heated natural samples, that cation ordering causes a significant decrease in the  $c$  lattice parameter. Novák *et al.* (2004) also pointed

\* E-mail: michele.zema@unipv.it

DOI: 10.1180/0026461067030335

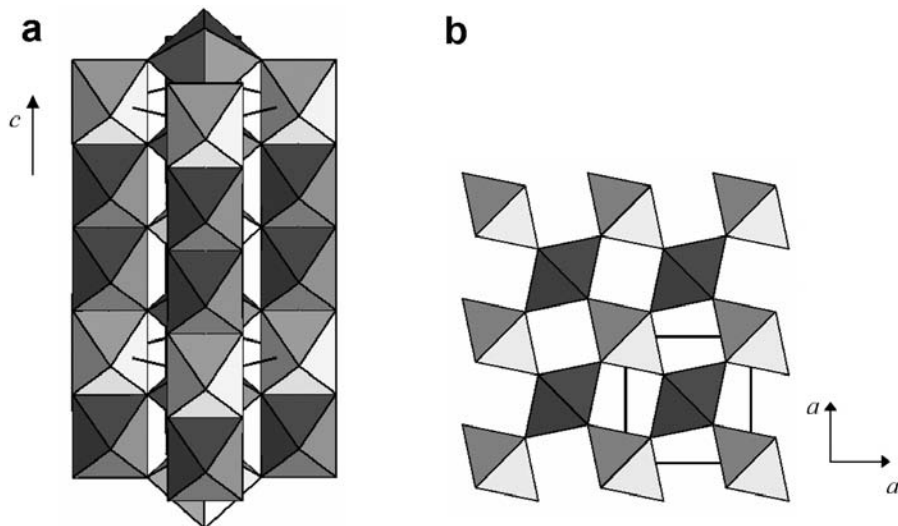


FIG. 1. The crystal structure of tapiolite viewed along (a) [110] and (b) [001].

out that differences in unit-cell dimensions have to be attributed to highly variable degrees of cation order by analysing different tapiolite samples from the Laštovičky lepidolite pegmatite.

According to Hansen *et al.* (1995), X-ray crystallography may lead to erroneous structural models in the case of partially disordered trirutile structures since trirutile can simply be described as commensurately modulated rutile by a sinusoidal scattering density wave added to the basic rutile structure along  $c$ . As a result, an infinite number of pairs of crystal structures (characterized by opposite degrees of cation order and different bond distances) should exhibit identical XRD patterns. They concluded that the structural model emerging from least-squares calculations will strongly depend on the starting point of the refinement.

In the present work, different structural states corresponding to different degrees of order, obtained by thermal treatment of single crystals of a natural tapiolite sample, have been analysed by means of XRD. Calibrations of the degree of order based on variations of the  $c$  dimension as well as of other structural parameters are presented and discussed.

## Experimental

### Samples

The sample used for the present study is a ferrotapiolite from Kimito (Finland), which was

kindly provided by the Mineralogical Museum of the University of Rome (sample inv. No. 10221/3). The XRD study was carried out on different single crystals. After the preliminary SC-XRD study, the selected crystals were submitted to *ex situ* annealing experiments in order to reach different ordering states. Annealing experiments were performed in sealed quartz vials under vacuum using a vertical furnace. At the end of each annealing run, crystals were quenched and a new SC-XRD analysis was performed to determine the degree of order and calculate all the relevant geometrical parameters.

### Electron microprobe analyses

The ferrotapiolite from Kimito was analysed at the Department of Earth Sciences of the University of Modena using an ARL-SEM-Q electron microprobe operating in the wavelength dispersive (WDS) mode. Operating conditions were 15 kV and 20 nA sample current. The counting times were 20 s for peak and 5 s for background. The standards used were: Nb metal (Nb- $L\alpha$ ), Ta metal (Ta- $M\alpha$ ), ilmenite (Fe- $K\alpha$ , Ti- $K\alpha$ ), Sc metal (Sc- $K\alpha$ ), spessartine (Mn- $K\alpha$ ), cassiterite (Sn- $L\alpha$ ), anorthite (Ca- $K\alpha$ ), W metal (W- $M\alpha$ ). X-ray counts were converted into oxide weight percentages using the PROBS correction program (Donovan and Rivers, 1990). Analyses are precise to within 1% for major elements and 3–5% for minor elements. Only the spot analyses which satisfied the following

STRUCTURAL CHANGES IN FERROTAPIOLITE

TABLE 1. Electron microprobe analysis of ferrotapiolite from Kimito.

Wt.% oxides		a.p.f.u. (based on 6 oxygen atoms)	
MnO	1.52(6)	Mn	0.112(4)
FeO	12.70(13)	Fe	0.920(13)
TiO <sub>2</sub>	0.44(4)	Ti	0.029(2)
Sc <sub>2</sub> O <sub>3</sub>	0.25(2)	Sc	0.019(2)
CaO	0.01(1)	Ca	0.003(5)
SnO <sub>2</sub>	1.00(10)	Sn	0.035(4)
Ta <sub>2</sub> O <sub>5</sub>	81.27(84)	Ta	1.799(16)
WO <sub>3</sub>	0.04(10)	W	0.001(3)
Nb <sub>2</sub> O <sub>5</sub>	3.16(49)	Nb	0.124(17)
Total	100.39(43)	Total	3.041(9)

Standard deviations are given in parentheses.

conditions were averaged: (1) total oxide amount = 100±1.5; (2) total cation content = 3.000±0.01 atoms on the basis of six oxygen atoms. The

chemical analysis and the formula calculated on the basis of six oxygen atoms for the ferrotapiolite sample are given in Table 1.

TABLE 2. Unit-cell parameters for untreated and heated tapiolite samples.

Crystal	Thermal treatment	Label	<i>a</i> (Å)	<i>c</i> (Å)	<i>V</i> (Å <sup>3</sup> )
Kim1	untreated	Kim1_q0	4.7533(4)	9.2876(10)	209.84(5)
Kim5	untreated	Kim5_q0	4.7533(3)	9.2773(7)	209.61(4)
	750°C 30 min	Kim5_q1	4.7554(11)	9.2281(22)	208.68(15)
Kim9	untreated	Kim9_q0	4.7531(5)	9.2873(10)	209.82(6)
	700°C 210 min	Kim9_q1	4.7475(4)	9.2690(8)	208.91(5)
	750°C 120 min	Kim9_q2	4.7497(8)	9.2530(16)	208.74(10)
	750°C 180 min	Kim9_q3	4.7504(4)	9.2549(8)	208.85(5)
Kim14	untreated	Kim14_q0	4.7551(3)	9.2810(7)	209.85(5)
	600°C 20 min	Kim14_q1	4.7526(4)	9.2501(9)	208.93(6)
Kim19	untreated	Kim19_q0	4.7561(5)	9.2748(11)	209.80(7)
	750°C 40 min	Kim19_q1	4.7516(4)	9.2258(8)	208.30(5)
	750°C 80 min	Kim19_q2	4.7531(4)	9.2219(7)	208.34(5)
Kim20	untreated	Kim20_q0	4.7561(4)	9.2880(8)	210.10(5)
	600°C 5 min	Kim20_q1	4.7547(5)	9.2893(10)	210.01(6)
	600°C 20 min	Kim20_q2	4.7516(4)	9.2856(8)	209.65(5)
	600°C 50 min	Kim20_q3	4.7509(4)	9.2811(7)	209.48(5)
	600°C 200 min	Kim20_q4	4.7509(4)	9.2812(8)	209.49(5)
	600°C 650 min	Kim20_q5	4.7506(5)	9.2811(10)	209.46(6)
	650°C 15 min	Kim20_q6	4.7507(4)	9.2794(8)	209.43(5)
Kim23	untreated	Kim23_q0	4.7551(4)	9.2818(8)	209.87(6)
	750°C 130 min	Kim23_q1	4.7538(4)	9.2193(7)	208.34(5)
	750°C 190 min	Kim23_q2	4.7571(7)	9.2189(14)	208.62(9)
Kim24	untreated	Kim24_q0	4.7562(4)	9.2910(7)	210.18(5)
	700°C 30 min	Kim24_q1	4.7499(3)	9.2716(7)	209.18(5)
	700°C 120 min	Kim24_q2	4.7511(3)	9.2648(7)	209.13(5)
	700°C 450 min	Kim24_q3	4.7561(5)	9.2030(11)	208.17(7)

Standard deviations are given in parentheses.

*X-ray single-crystal diffraction*

Intensity data were obtained at room temperature on a Bruker AXS Smart Apex three-circle diffractometer equipped with a CCD detector using graphite monochromatized Mo- $K\alpha$  radiation ( $\lambda = 0.71073 \text{ \AA}$ ). Data were collected at operating conditions of 50 kV and 30 mA. The Bruker SMART system of programs was used for preliminary crystal-lattice determination and X-ray data collection. For each crystal, a total of 3340 frames (resolution:  $512 \times 512$  pixels) were collected with four different goniometer settings ( $\varphi = 0^\circ, 90^\circ, 180^\circ, 270^\circ$ ) using the  $\omega$ -scan mode (scan width:  $0.2^\circ\omega$ ; exposure time: 5 s/frame; detector-sample distance: 4 cm). Completeness of measured data was achieved up to  $39^\circ\theta$ . The Bruker program SAINT+ was used for the data

reduction including intensity integration, background and Lorentz-polarization corrections. Final unit-cell parameters were obtained by the Bruker GLOBAL least-squares orientation matrix refinement procedure based on the positions of all measured reflections and are reported in Table 2 for all the analysed crystals. The semi-empirical absorption correction of Blessing (1995), based on the determination of transmission factors for equivalent reflections, was applied using the Bruker program SADABS. A further correction for spherical absorption was attempted but no improvement to the datasets in terms of internal agreement factors was achieved. Details on data collections are reported in Table 3.

The values of equivalent reflections were averaged and the resulting discrepancy factors are reported in Table 3. Structure refinements

TABLE 3. Details on X-ray data collections and structure refinements.

	$I_{\text{tot}}$	$I_{\text{ind}}$	$R_{\text{int}}$ (%)	$R$ (%)	$wR$ (%)	$S$
Kim1_q0	4225	341	4.78	4.65	5.96	1.131
Kim5_q0	4196	336	4.15	2.92	5.47	1.240
Kim5_q1	3596	340	4.93	3.54	6.12	1.002
Kim9_q0	4192	344	4.28	4.06	7.47	1.283
Kim9_q1	4135	343	4.64	2.96	6.56	1.222
Kim9_q2	4140	339	5.00	3.31	5.39	1.015
Kim9_q3	4158	344	5.42	3.04	6.21	1.219
Kim14_q0	4173	348	3.57	3.06	5.47	1.254
Kim14_q1	4084	336	4.21	2.55	3.81	1.293
Kim19_q0	3939	342	5.40	4.25	7.46	1.016
Kim19_q1	3930	343	5.94	3.85	6.94	0.724
Kim19_q2	3906	345	6.27	3.58	6.73	1.101
Kim20_q0	4242	339	3.91	3.05	5.50	1.339
Kim20_q1	4206	340	5.21	4.09	4.11	1.264
Kim20_q2	4218	345	3.96	3.55	6.31	1.209
Kim20_q3	4213	345	5.37	3.93	6.12	1.260
Kim20_q4	4223	341	4.46	3.07	4.93	1.342
Kim20_q5	4218	341	4.02	3.08	4.71	1.297
Kim20_q6	4209	338	4.43	3.35	4.90	1.263
Kim23_q0	4161	339	5.23	4.81	4.22	1.004
Kim23_q1	3937	342	6.84	4.29	8.00	1.162
Kim23_q2	3988	342	7.08	4.49	8.57	1.149
Kim24_q0	4200	341	4.87	3.59	7.06	1.004
Kim24_q1	4176	343	4.52	2.61	5.05	1.032
Kim24_q2	4124	337	5.55	2.63	5.00	1.147
Kim24_q3	4109	339	4.99	1.85	3.64	1.273

$R_{\text{int}} = \Sigma |F_o^2 - F_o^2(\text{mean})| / \Sigma [F_o^2]$ ;  $R_{\text{all}} = \Sigma ||F_o| - |F_c|| / \Sigma [F_o]$ ;  $S = [\Sigma [w(F_o^2 - F_c^2)^2] / (n-p)]^{0.5}$ , where  $n$  is the number of reflections and  $p$  is the total number of parameters refined.  $I_{\text{tot}}$  is the total number of reflections after merging identical reflections (redundancy of measurements was  $\sim 1.3$ );  $I_{\text{ind}}$  is the number of independent reflections used for structure refinements. All datasets from crystals Kim19 and Kim23 were refined with isotropic displacement parameters. For all the other samples a total of 34 parameters was refined.

## STRUCTURAL CHANGES IN FERROTAPIOLITE

were carried out in space group  $P4_2/mnm$  using the program *Crystals* (Betteridge *et al.*, 2003). The atomic scattering curves were taken from the *International Tables for X-ray Crystallography* (Ibers and Hamilton, 1974). Structure factors were weighted according to the Chebichev schemes (Carruthers and Watkin, 1979). Taking into account the observations of Hansen *et al.* (1995), different starting models, obtained by changing site occupancies of *A* and *B* sites and atomic coordinates of oxygen atoms, were used for each refinement. In the first stages of least-squares refinement, only scale factor and atomic coordinates were refined. Anisotropic displacement parameters, site occupancies of cation sites and an isotropic extinction parameter (Larson, 1970) were added to the refinement in subsequent cycles. In the last cycles of refinements, all parameters were refined simultaneously. The following restraints were used: (1) all structural

sites were considered fully occupied; (2) total Fe content  $X_{Fe}^A + 2X_{Fe}^B = 1$ . For all the crystals, the small amount of  $Nb^{5+}$  present in this sample (see chemical analysis) was inserted in the *B* site and not refined. Final discrepancy factors, together with the goodness of fit *S* and the number of total and unique reflections  $I_{tot}$  and  $I_{ind}$ , are reported in Table 3. Final site occupancies are reported in Table 4.

It is worth noting that different starting models led to different results with final discrepancy factors not much larger than the one given by the actual minimum. Besides discrepancy factor differences, geometric considerations allowed us to recognize false minima.

The order parameter used here to describe the degree of Fe/Ta order between *A* and *B* sites is taken as  $Q = |X_{Fe}^A - X_{Fe}^B| = |X_{Ta}^B - X_{Ta}^A|$ , where  $X_{Fe}^A$  and  $X_{Fe}^B$  represent the site occupancies of  $Fe^{2+}$  occupying the *A* and *B* sites, respectively, and

 TABLE 4. Mean atomic numbers (m.a.n.), site occupancies and *Q* values.

	m.a.n. <i>A</i> Site	m.a.n. <i>B</i> Site	m.a.n. <i>A</i> +2 <i>B</i>	$Fe^{2+}(A)$	$Ta^{5+}(A)$	$Fe^{2+}(B)$	$Ta^{5+}(B)$	<i>Q</i>
Kim1_q0	52.51(19)	57.67(9)	167.84(28)	0.436(4)	0.564(4)	0.282(2)	0.653(2)	0.154
Kim5_q0	48.37(19)	59.75(9)	167.86(28)	0.524(4)	0.476(4)	0.238(2)	0.697(2)	0.286
Kim5_q1	38.46(33)	64.71(19)	167.89(50)	0.735(7)	0.265(7)	0.132(4)	0.803(4)	0.603
Kim9_q0	52.56(24)	57.62(9)	167.79(35)	0.435(5)	0.565(5)	0.283(2)	0.652(2)	0.152
Kim9_q1	50.58(14)	58.64(9)	167.85(22)	0.477(3)	0.523(3)	0.261(2)	0.674(2)	0.216
Kim9_q2	48.51(19)	59.68(9)	167.86(28)	0.521(4)	0.479(4)	0.239(2)	0.696(2)	0.282
Kim9_q3	47.06(24)	60.39(9)	167.84(35)	0.552(5)	0.448(5)	0.224(2)	0.711(2)	0.328
Kim14_q0	48.84(19)	59.50(9)	167.84(28)	0.514(4)	0.486(4)	0.243(2)	0.692(2)	0.271
Kim14_q1	40.48(24)	63.68(9)	167.84(35)	0.692(5)	0.308(5)	0.154(2)	0.781(2)	0.538
Kim19_q0	46.30(24)	60.77(14)	167.84(37)	0.568(5)	0.432(5)	0.216(3)	0.719(3)	0.352
Kim19_q1	37.99(24)	64.95(14)	167.89(37)	0.745(5)	0.255(5)	0.127(3)	0.808(3)	0.618
Kim19_q2	36.28(28)	65.77(19)	167.83(44)	0.781(6)	0.219(6)	0.110(4)	0.826(4)	0.672
Kim20_q0	50.35(14)	58.75(9)	167.85(22)	0.482(3)	0.518(3)	0.259(2)	0.676(2)	0.223
Kim20_q1	50.49(28)	58.70(14)	167.89(42)	0.479(6)	0.521(6)	0.260(3)	0.675(3)	0.219
Kim20_q2	49.42(19)	58.96(9)	167.84(28)	0.491(4)	0.509(4)	0.255(2)	0.681(2)	0.237
Kim20_q3	50.30(24)	58.75(9)	167.79(35)	0.483(5)	0.517(5)	0.259(2)	0.676(2)	0.224
Kim20_q4	49.50(24)	59.17(9)	167.84(35)	0.500(5)	0.500(5)	0.250(2)	0.685(2)	0.250
Kim20_q5	49.55(19)	59.15(9)	167.85(28)	0.499(4)	0.501(4)	0.250(2)	0.685(2)	0.249
Kim20_q6	49.41(24)	59.22(9)	167.84(35)	0.502(5)	0.498(5)	0.249(2)	0.686(2)	0.253
Kim23_q0	48.09(24)	59.88(14)	167.84(37)	0.530(5)	0.470(5)	0.235(3)	0.700(3)	0.295
Kim23_q1	36.25(52)	65.80(28)	167.84(79)	0.782(11)	0.218(11)	0.109(6)	0.826(6)	0.673
Kim23_q2	34.79(56)	66.50(28)	167.79(84)	0.813(12)	0.187(12)	0.094(6)	0.841(6)	0.719
Kim24_q0	51.47(14)	58.18(9)	167.83(22)	0.458(3)	0.542(3)	0.271(2)	0.664(2)	0.187
Kim24_q1	49.12(14)	59.35(9)	167.82(22)	0.508(3)	0.492(3)	0.246(2)	0.689(2)	0.262
Kim24_q2	47.71(14)	60.07(9)	167.84(22)	0.538(3)	0.462(3)	0.231(2)	0.704(2)	0.307
Kim24_q3	26.71(24)	70.59(14)	167.89(37)	0.985(5)	0.015(5)	0.007(3)	0.928(3)	0.978

Standard deviations are given in parentheses.

$Nb^{5+}$  occupancy at site *B* was fixed at 0.065 according to EMPA.

similarly for  $X_{\text{Ta}^*}^B$  and  $X_{\text{Ta}^*}^A$  ( $\text{Ta}^* = \text{Ta} + \text{Nb}$ ).  $Q$  values are reported in Table 4.

Bond distances and other geometrical parameters are given in Tables 5 and 6 for the *A* and *B* sites, respectively.

**Results and discussion**

*From rutile-type to trirutile-type structure*

Cation ordering in tapiolite induces a transformation from rutile-type to trirutile-type structure. Using the definition given by Goldschmidt (1926), these structures are related by a ‘polymeric isomorphism’, which can be viewed as putting three rutile unit cells, one on top of the other, and hence implies a tripling of the *c* cell parameter. In the following discussion, the tripled cell is always used to analyse the structural variations.

In Fig. 2, variations of lattice constants as a function of  $Q$  are shown. Data taken from the literature (Turnock, 1966; Kinast *et al.*, 2002; Wise and Černý, 1996; Mello *et al.*, 1999; Antonietti *et al.*, 2001; Novák *et al.*, 2004) on completely ordered ferrotapiolites are also

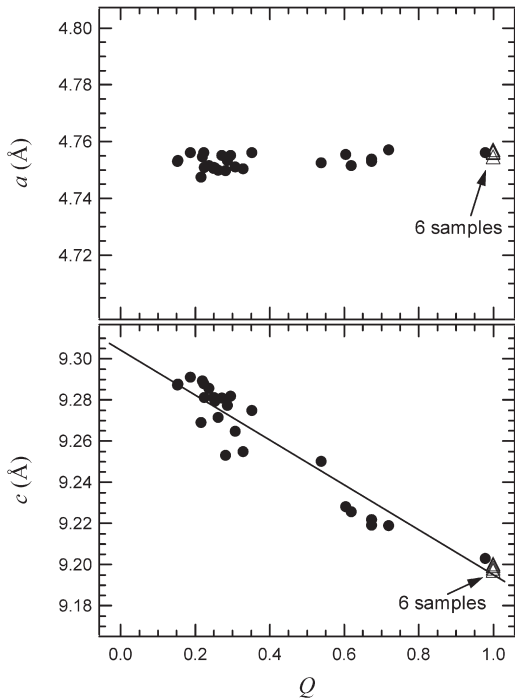


FIG. 2. Variation of unit-cell parameters as a function of  $Q$ . Solid circles: this study; open triangles: data from the literature (see text).

reported for comparison. As is evident from the figure, the *a* cell parameter does not vary significantly while the *c* cell parameter decreases linearly with increasing degree of order. Unweighted linear regression of all the data including those from the literature yields:

$$c \text{ (Å)} = 9.3042(26) - 0.1092(46) Q \text{ (} R=0.97 \text{)} \quad (1)$$

For a better evaluation of the variations of unit-cell dimensions with  $Q$ , the *a/c* ratio has also been considered:

$$a/c = 0.5105(1) - 0.0072(3) Q \text{ (} R=0.97 \text{)} \quad (2)$$

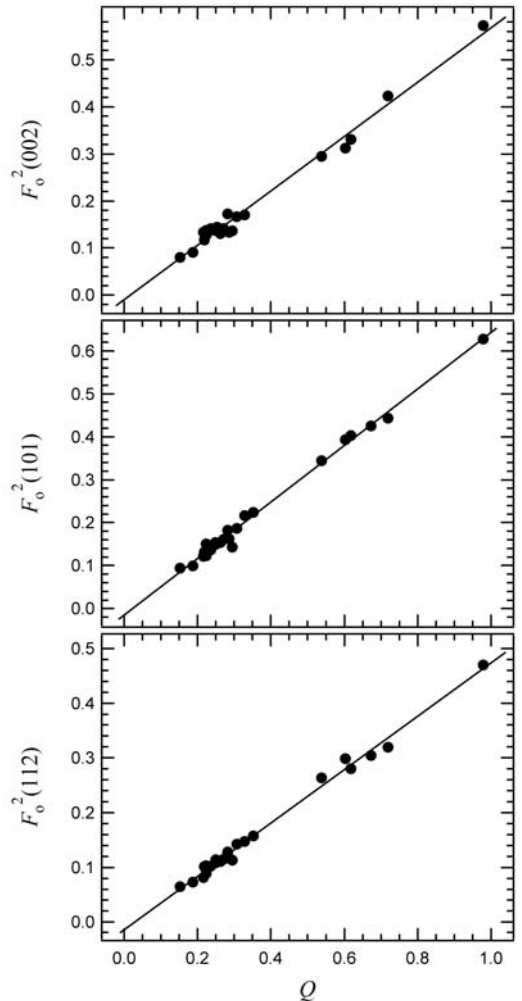


FIG. 3. Observed structure factors of the most intense supercell reflections normalized with respect to the  $F_o^2$  of reflections with  $l = 3n$  of the relative lattice rows as a function of  $Q$ .

TABLE 5. Bond distances (Å) and selected geometrical parameters for the *A* site.

	<i>A</i> -O1 (× 2)	<i>A</i> -O2 (× 4)	< <i>A</i> -O>	<i>V</i> <sub>A</sub>	OQ <i>E</i> <sub>A</sub>	OAV <sub>A</sub>	<i>asp</i>
Kim1_q0	2.037(6)	2.053(4)	2.048(5)	11.34	1.0079	27.96	1.169
Kim5_q0	2.044(4)	2.076(3)	2.065(3)	11.62	1.0076	26.60	1.162
Kim5_q1	2.072(6)	2.121(3)	2.104(4)	12.27	1.0085	29.17	1.170
Kim9_q0	2.025(5)	2.061(4)	2.049(4)	11.33	1.0085	29.62	1.171
Kim9_q1	2.034(4)	2.065(3)	2.055(3)	11.44	1.0074	25.89	1.159
Kim9_q2	2.037(5)	2.076(3)	2.063(4)	11.57	1.0080	27.93	1.166
Kim9_q3	2.044(4)	2.087(2)	2.073(3)	11.71	1.0091	31.61	1.178
Kim14_q0	2.040(5)	2.072(3)	2.061(3)	11.52	1.0086	30.33	1.174
Kim14_q1	2.058(4)	2.103(4)	2.088(3)	11.98	1.0086	29.66	1.172
Kim19_q0	2.056(5)	2.074(3)	2.068(4)	11.62	1.0096	33.77	1.184
Kim19_q1	2.058(6)	2.108(4)	2.091(4)	12.03	1.0091	31.39	1.177
Kim19_q2	2.075(3)	2.123(1)	2.107(2)	12.31	1.0092	31.76	1.178
Kim20_q0	2.037(3)	2.066(2)	2.056(2)	11.45	1.0086	30.14	1.173
Kim20_q1	2.025(10)	2.077(7)	2.060(8)	11.50	1.0087	29.83	1.172
Kim20_q2	2.023(4)	2.077(3)	2.059(3)	11.49	1.0084	28.57	1.168
Kim20_q3	2.020(5)	2.071(4)	2.054(4)	11.41	1.0083	28.67	1.168
Kim20_q4	2.033(5)	2.078(4)	2.063(4)	11.57	1.0079	27.16	1.163
Kim20_q5	2.038(5)	2.079(4)	2.065(4)	11.61	1.0083	28.75	1.169
Kim20_q6	2.025(6)	2.070(4)	2.055(5)	11.43	1.0082	28.23	1.167
Kim23_q0	2.028(5)	2.090(4)	2.069(4)	11.64	1.0097	33.13	1.182
Kim23_q1	2.069(4)	2.130(2)	2.110(3)	12.35	1.0092	31.41	1.177
Kim23_q2	2.096(5)	2.136(3)	2.123(4)	12.60	1.0084	29.44	1.171
Kim24_q0	2.047(4)	2.059(3)	2.055(3)	11.42	1.0088	31.04	1.176
Kim24_q1	2.045(3)	2.072(2)	2.063(2)	11.57	1.0079	27.67	1.165
Kim24_q2	2.042(4)	2.081(2)	2.068(3)	11.66	1.0080	27.81	1.166
Kim24_q3	2.096(2)	2.142(2)	2.127(2)	12.63	1.0100	34.57	1.187

Standard deviations are given in parentheses.

The equation above represents a unique tool for a quick evaluation of the degree of order of tapiolite samples after only the lattice constants have been determined. Although the tapiolite compositional range is rather narrow, data from other tapiolite samples of different Fe, Ta and minor element contents would be useful for a better and more generally valid evaluation of order parameters from lattice constants.

Another quick and direct measure of the degree of order can be gained from the intensities of supercell reflections. Such reflections, characterized by  $l \neq 3n$ , arise as a consequence of the tripling of the unit cell and are expected to gain intensity as sites differentiate due to Fe-Ta ordering. In Fig. 3, the  $F_o^2$  of the most intense supercell reflections of the tapiolite structure, each normalized with respect to the  $F_o^2$  of reflections with  $l = 3n$  and belonging to the same lattice row, are reported as a function of  $Q$ . As is evident from the graph, the trends are fairly

linear in all cases. All the measured reflections remained sharp showing no significant changes in profile shape during the ordering process.

#### Geometrical variations

As already stated, in the completely disordered state, the tapiolite structure transforms into the rutile aristotype; thus the *A* and *B* sites merge into a single octahedron. As long as the ordering process takes place, the two sites, now distinct from a crystallographic point of view, become more and more different. In particular, this is evident from Fig. 4 where the mean cation-oxygen distances are reported. The two mean bond lengths converge into a single value at an order degree close to zero (within the resolution of our measurement), and with increasing  $Q$  the *A* site becomes larger due to the entrance of the larger Fe<sup>2+</sup> ion (i.r. 0.78 Å; Shannon, 1976) while the *B* site becomes smaller (Ta<sup>5+</sup> i.r. 0.64 Å).

TABLE 6. Bond distances (Å) and selected geometrical parameters for the  $B$  site.

	$B-O1$ ( $\times 2$ )	$B-O2$ ( $\times 2$ )	$B-O2$ ( $\times 2$ )	$\langle B-O \rangle$	$V_B$	$OQE_B$	$OAV_B$	$Ct_B-B$
Kim1_q0	2.040(4)	2.027(5)	2.032(4)	2.033(4)	11.08	1.0071	25.06	0.0033
Kim5_q0	2.037(2)	2.007(2)	2.030(2)	2.024(2)	10.95	1.0065	23.01	0.0068
Kim5_q1	2.019(4)	1.986(3)	2.000(3)	2.002(3)	10.60	1.0057	20.14	0.0141
Kim9_q0	2.047(3)	2.023(4)	2.029(4)	2.033(4)	11.09	1.0066	23.30	0.0028
Kim9_q1	2.038(3)	2.008(3)	2.033(3)	2.026(3)	10.99	1.0066	23.20	0.0051
Kim9_q2	2.037(3)	2.007(3)	2.020(3)	2.021(3)	10.91	1.0061	21.39	0.0075
Kim9_q3	2.034(3)	2.008(3)	2.008(3)	2.017(3)	10.84	1.0060	21.23	0.0086
Kim14_q0	2.040(3)	2.019(3)	2.022(3)	2.027(3)	10.99	1.0066	23.31	0.0061
Kim14_q1	2.028(3)	1.996(3)	2.007(3)	2.010(3)	10.74	1.0059	20.93	0.0124
Kim19_q0	2.030(3)	2.026(4)	2.010(3)	2.022(3)	10.90	1.0071	25.23	0.0070
Kim19_q1	2.025(4)	1.996(5)	1.996(4)	2.006(4)	10.67	1.0056	19.76	0.0127
Kim19_q2	2.016(2)	1.988(2)	1.990(2)	1.998(2)	10.54	1.0059	20.78	0.0150
Kim20_q0	2.042(2)	2.023(3)	2.026(2)	2.030(2)	11.04	1.0068	24.02	0.0045
Kim20_q1	2.049(7)	2.014(6)	2.026(6)	2.030(6)	11.05	1.0060	21.07	0.0042
Kim20_q2	2.050(3)	2.009(3)	2.027(3)	2.029(3)	11.04	1.0060	20.84	0.0054
Kim20_q3	2.051(3)	2.013(5)	2.027(4)	2.030(4)	11.06	1.0060	21.15	0.0054
Kim20_q4	2.042(3)	2.005(4)	2.030(4)	2.026(4)	10.98	1.0062	21.74	0.0058
Kim20_q5	2.039(3)	2.008(4)	2.025(3)	2.024(3)	10.95	1.0064	22.45	0.0059
Kim20_q6	2.047(4)	2.012(4)	2.027(4)	2.029(4)	11.03	1.0062	21.77	0.0059
Kim23_q0	2.048(3)	2.013(6)	2.012(4)	2.024(4)	10.97	1.0056	19.79	0.0064
Kim23_q1	2.020(2)	1.984(3)	1.990(3)	1.998(3)	10.54	1.0055	19.43	0.0151
Kim23_q2	2.005(3)	1.978(4)	1.994(3)	1.992(3)	10.44	1.0063	22.34	0.0165
Kim24_q0	2.036(2)	2.030(3)	2.025(3)	2.030(3)	11.03	1.0075	26.66	0.0039
Kim24_q1	2.034(2)	2.011(2)	2.027(2)	2.024(2)	10.93	1.0067	23.66	0.0063
Kim24_q2	2.036(2)	2.005(2)	2.022(2)	2.021(2)	10.90	1.0062	21.74	0.0076
Kim24_q3	2.003(1)	1.981(2)	1.973(1)	1.986(1)	10.34	1.0064	22.83	0.0197

Standard deviations are given in parentheses.  $Ct_B$  is the centroid of the  $B$  polyhedron

Octahedral distortion parameters,  $OQE$  and  $OAV$  (Robinson *et al.*, 1971), for both the sites

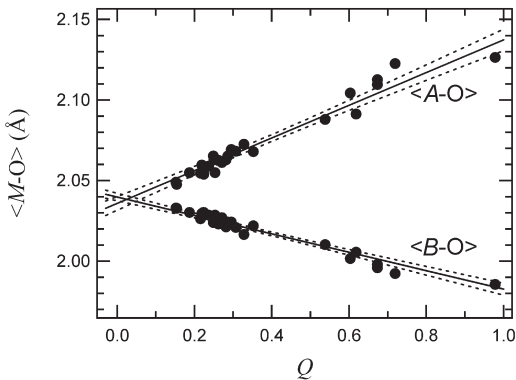


FIG. 4. Variation of mean cation–oxygen distances as a function of  $Q$  for  $A$  and  $B$  sites. Solid lines: weighted linear fit to the data; areas between dotted lines: confidence bands, with confidence interval of 95%.

(see data in Tables 5 and 6) are characterized by fairly low values and do not change significantly with increasing  $Q$  indicating that the polyhedra are almost regular along the whole  $Q$  range. The  $A$  site shows a little tetragonal distortion with the axial bond distances ( $A-O1$ ) shorter than the equatorial ones ( $A-O2$ ), the difference increasing with the degree of order (see data in Tables 5 and 6). The deviation from the ideal quadratic ‘basal plane’ of the  $A$  octahedron has been calculated for all the analysed samples by the aspect ratio ( $asp$ ), which is defined as  $(O2-O2//c \text{ axis})/(O2-O2// (110) \text{ face})$  (Riss *et al.*, 2003), and ranges between 1.16 and 1.18 (see data in Table 5).

With regard to the relative position of the cations inside the polyhedra, the cation at site  $A$  is constrained to lie on  $\bar{1}$ -symmetry position (this cancels the cation-cation repulsion along the chain), i.e. at the origin of the unit cell, which corresponds to the barycentre of the polyhedron itself. The  $B$  cation is instead free to move along

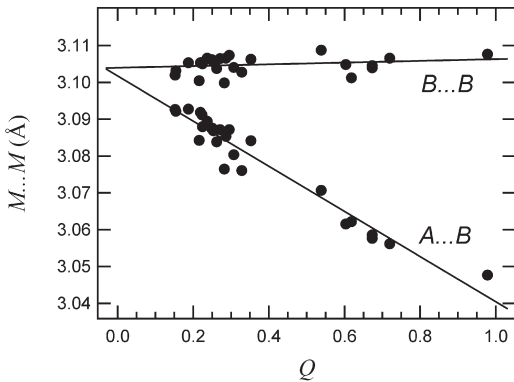


FIG. 5. Cation–cation distances measured along the chain.

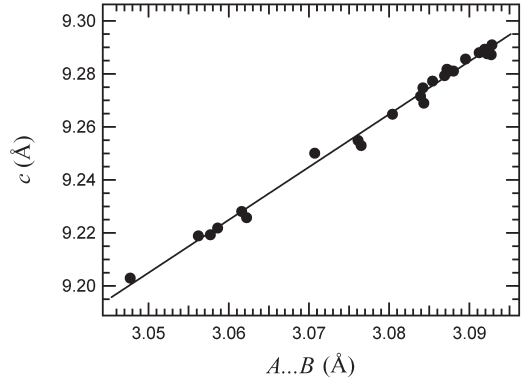


FIG. 7. Linear correlation between the  $c$  lattice parameter and  $A\cdots B$  distance along the chain.

the  $c$  axis. Such movement allows an offset displacement of the cation from the centroid (Ct) of the polyhedron (see  $Ct_B-B$  distances in Table 6).

Along the  $\dots ABBABB\dots$  chain, the  $B\cdots B$  segment remains rigid and fixed to the value of  $3.104(1)$  Å which corresponds to the  $c$  cell parameter of the rutile-type monomer, as can be derived by using equation 1. On the other hand, the  $A\cdots B$  distance, obviously starts from the same value at  $Q = 0$  and decreases linearly with increasing ordering, as shown in Fig. 5. The  $z/c$  coordinate of the  $B$  position moves linearly towards the origin of the unit cell, as shown in Fig. 6. The extrapolated value of the  $z/c$  coordinate at  $Q = 0$  is 0.333, as expected. This is a further confirmation of the reliability of the results of our structure refinements. It is worth noting that the  $A\cdots B$  distance is responsible for

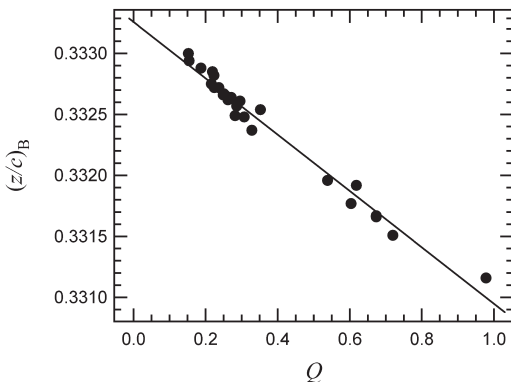


FIG. 6. Displacement of the  $B$  site position as a function of  $Q$ .

the  $c$  lattice parameter decreasing with  $Q$ , as shown by the perfectly linear relationship between these two parameters reported in Fig. 7.

### Acknowledgements

The authors thank O. Grubessi and L. Marino (University of Rome) for providing the sample and are grateful to S. Bigi and for funding by the Department of Earth Sciences of University of Modena for the microprobe analyses. Comments by M. Tribaudino and an anonymous reviewer are acknowledged. Financial support was provided by the Italian MIUR project 'Mineral physics and technological applications of the columbite-tantalite-tapiolite system'.

### References

- Antonietti, V., Kinast, E.J., Zawislak, L.I., da Cunha and dos Santos, C.A. (2001) Structure refinement of mixed oxides  $(Fe_xCo_{1-x})Ta_2O_6$ . *Journal of Physics and Chemistry of Solids*, **62**, 1239–1242.
- Baur, W.H. (1994) Rutile type derivatives. *Zeitschrift für Kristallographie*, **209**, 143–150.
- Betteridge, P.W., Carruthers, J.R., Cooper, R.I., Prout, K. and Watkin, D.J. (2003) *CRYSTALS* version 12: software for guided crystal structure analysis. *Journal of Applied Crystallography*, **36**, 1487.
- Blessing, R.H. (1995) An empirical correction for absorption anisotropy. *Acta Crystallographica*, **A51**, 33–38.
- Carruthers, J.R. and Watkin, D.J. (1979) Chebychev Weighting. *Acta Crystallographica*, **A35**, 698–699.
- Donovan, J.J. and Rivers, M.L. (1990) PRSUPR – A PC Based Automation and Analysis Software Package

- for Wavelength-Dispersive Electron-Beam Microanalysis. *Microbeam Analysis*, 66–68.
- Goldschmidt, V.M. (1926) Geochemische Verteilungsgesetze der Elemente. VI. Über die Kristallstrukturen vom Rutiltypus mit Bemerkungen zur Geochemie Zweiwertiger und Vierwertiger Elemente. *Videnskapselskapets Academii i Oslo I, Math.-Naturv. Klasse, Skrifter*, **1**, 5–21.
- Hansen, S., Landa-Cánovas, A., Ståhl, K. and Nilsson, J. (1995) Cation ordering waves in trirutiles. When X-ray crystallography fails? *Acta Crystallographica*, **A51**, 514–519.
- Ibers, J.A. and Hamilton, W.C. (1974) *International Tables for X-ray Crystallography*. Kynoch Press, Birmingham, UK, vol. **4**, pp. 99–101.
- Kinast, E.J., Zawislak, L.I., da Cunha, J.B.M., Antonietti, V., de Vasconcelos, M.A.Z. and dos Santos, C.A. (2002) Coexistence of rutile and trirutile phases in a natural tapiolite sample. *Journal of Solid State Chemistry*, **163**, 218–223.
- Larson, A.C. (1970) The inclusion of secondary extinction in least-squares refinement of crystal structures. Pp. 291–294 in: *Crystallographic Computing* (F.R. Ahmed, S.R. Hall and C.P. Huber, editors). Munksgaard, Copenhagen.
- Mello, V.D., Zawislak, L.I., da Cunha, J.B.M., Kinast, E.J., Soares, J.B. and dos Santos, C.A. (1999) Structure and magnetic properties of layered  $(\text{Fe}_x\text{Co}_{1-x})\text{Ta}_2\text{O}_6$  compounds. *Journal of Magnetism and Magnetic Materials*, **196–197**, 846–847.
- Novák, M., Černý, P., Cempírek, J., Šrein, V. and Filip, J. (2004) Ferrotapiolite as a pseudomorph of stibiotantalite from the Laštovičky lepidolite pegmatite, Czech Republic; an example of hydrothermal alteration at constant Ta/(Ta+Nb). *The Canadian Mineralogist*, **42**, 1117–1128.
- Riss, A., Blaha, P., Schwarz, K. and Zeeman, J. (2003) Theoretical explanation of the octahedral distortion in  $\text{FeF}_2$  and  $\text{MgF}_2$ . *Zeitschrift für Kristallographie*, **218**, 585–589.
- Robinson, K., Gibbs, G.V. and Ribbe, P.H. (1971) Quadratic elongation, a quantitative measure of distortion in co-ordination polyhedra. *Science*, **172**, 567–570.
- Shannon, R.D. (1976) Revised effective ionic radii and systematic studies of interatomic distances in halides and chalcogenides. *Acta Crystallographica*, **A32**, 751–767.
- Turnock, A.C. (1966) Synthetic wadginite, tapiolite and tantalite. *The Canadian Mineralogist*, **8**, 461–470.
- Wise, M.A. and Černý, P. (1996) The crystal chemistry of the tapiolite series. *The Canadian Mineralogist*, **34**, 631–647.

[Manuscript received 17 February 2006;  
revised 23 May 2006]